

On the Modelling of Perfusion in the Simulation of RF-Ablation

Tobias Preusser* Andreas Weihusen[†] Heinz-Otto Peitgen[†]

Abstract

We compare three different strategies for the modelling of blood-perfusion in large vessels in a well known mathematical model for the simulation of radio-frequency ablation of tumors. The first approach models the perfusion with a heat-sink on the right hand side of the bioheat-transfer equation, the second approach considers the temperature to be fixed to the body-temperature and thus sets a Dirichlet boundary condition in the vessels. In the last approach we model the perfusion by increasing the effective diffusivity. The models are discretized using a standard finite element approach. The paper gives a review of the general model, the FE discretization, and finally compares results of the three perfusion modelling approaches on artificial and real data sets.

1 Introduction

The simulation of radio-frequency (RF) ablation for the treatment of malignant lesions is an indispensable tool for the planning of this treatment: A mono- or bi-polar internally cooled probe is placed into the malignant tissue. From the probe an electric current flows through the body and heats the tissue due to its electric resistance. Consequently cells are heated and their proteins coagulate. Finally this results in a volume of destroyed tissue, which in the case of success includes the malignant lesion.

The simulation of the treatment can provide a dosimetry planning, i.e. it can give hints where to place the probe, which power to apply and how long the current should be flowing. Such a simulation model reflects the (bio-)physical and chemical processes which are involved. Special emphasis has to be put in the modelling of blood-flow (perfusion), since the vessels act as cooling devices. Indeed, it can be impossible to completely destroy a lesion in the vicinity of large vessels. In the interest of the patient a simulation can help to decide whether a lesion is destructible by RF-ablation or not.

The idea of simulating the RF ablation has been tracked by several researchers. Some use commercial grid generators and finite element software [TSHea02]. Others have build their own model and discretized it with finite difference approaches [Ste00]. In the literature one finds several approaches for the modelling of the above mentioned blood-perfusion [Ste00, Pen48, JGG79].

This paper compares three of these approaches to the modeling of the blood perfusion. In Section 2 we review the general simulation model and in Section 3 we then discuss the

*CeVis, University of Bremen, Universitätsallee 29, 28359 Bremen, Germany

[†]MeVis, University of Bremen, Universitätsallee 29, 28359 Bremen, Germany

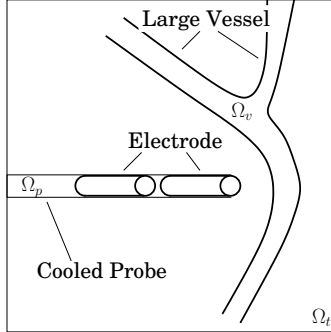


Figure 1: Configuration of computational domain Ω which contains the RF-probe Ω_p and large vessels Ω_v .

perfusion models. After briefly describing the discretization of the models in Sections 4 and 5 we present their application to artificial vascular data as well as vascular trees resulting from real CT scans. Finally we draw conclusions and discuss future work in Section 7.

2 A mathematical model for RF ablation

Our model for the simulation of the RF ablation is based on the work of Stein [Ste00]. It consists basically of three parts which act simultaneously and interfere with each other: First, the energy, which is applied to the tissue, must be computed. This is done by the calculation of the electric current emerging from the RF-probe. Second, this electric current heats the tissue due to its electric (Ohm) resistance. The heat diffuses into areas distant from the probe. But at the same time the circulating blood cools the tissue, particularly in the vicinity of large vessels. Moreover at larger temperatures the vaporization of nitrogen and water influence the energy balance. Third, the heat effects the proteins in the tissue-cells. The proteins coagulate and consequently the (malignant) cells die.

The three parts of the RF ablation model we have identified above depend on a variety of material parameters ranging from the electrical and thermal tissue properties to the biochemical properties of the proteins. Moreover these tissue parameters depend nonlinearly on the frequency f of the induced electric current, the temperature of the tissue T , its water content and the state of protein-coagulation. Finally, the material properties incorporate hystereses, i.e. tissue which has been heated and is cooled down again behaves differently as in its native state.

In the next paragraphs we review the model developed by Stein [Ste00] in more detail. For the simplicity of the presentation we reduce the nonlinearity of the model by considering material parameters to be constant. We refer the reader to the original work of Stein [Ste00] for details on the variability of the material properties.

The configuration

Let us consider a three dimensional domain $\Omega \subset \mathbb{R}^3$. In this work the focus lies on the cooling effects of vascular structures, thus we assume the domain to decompose into $\Omega = \Omega_v \cup \Omega_p \cup \Omega_t$, where Ω_v denotes the vascular structures, Ω_p the RF-probe and Ω_t the functional tissue (cf. Figure 1). We consider the probe to contain two electrodes (i.e. the probe is bipolar), which we denote $\Gamma^\pm \subset \Omega_p$ and to be internally cooled.

The aim is to find the distribution of temperature $T : [0, \infty) \times \Omega \rightarrow \mathbb{R}$ over the parabolic cube $Q := [0, \infty) \times \Omega$. For any time $t \in [0, \infty)$ and any spatial point $x \in \Omega$ we are looking for the temperature $T(t, x)$ at this point $(t, x) \in Q$.

Electric potential

Since the frequency of the electric current is $f = 500\text{KHz}$, the electromagnetic field, respectively the electric potential can be considered quasi-static [Ste00] and thus not depending on the time t . Consequently we do not have to consider the full Maxwell-Equations but only the electrostatic equation to obtain the potential $P : \Omega \rightarrow \mathbb{R}$:

Find $P : \Omega \rightarrow \mathbb{R}$ such that

$$\begin{aligned} -\operatorname{div}(\sigma(x)\nabla P(x)) &= 0 && \text{in } \Omega_t, \\ \partial_n P(x) &= 0 && \text{on } \partial\Omega, \\ P(x) &= g^\pm(x) && \text{on } \Gamma^\pm. \end{aligned} \tag{1}$$

Above, g^\pm is the potential applied by the external generator to the electrodes Γ^\pm . At the boundary of the domain Ω we consider Neumann conditions; ∂_n denotes the derivative with respect to the outer normal to Ω . And the material parameter $\sigma(x)$ denotes the electric conductivity of the tissue.

Heat distribution

The electric current induced by the quasi-static potential P heats the tissue due to the electric resistance of the cells. Furthermore this heat-energy diffuses away from the source (= the probe) a fact which is modelled by the well known heat-equation (in this context also referred to as the bioheat-transfer-equation) with appropriate source terms:

Find $T : [0, \infty) \times \Omega \rightarrow \mathbb{R}$ such that

$$\begin{aligned} \partial_t T(t, x) - \operatorname{div}(\lambda(x)\nabla T(t, x)) &= q(t, x) && \text{in } [0, \infty) \times \Omega_t, \\ T(t, x) &= T_{\text{probe}} && \text{in } [0, \infty) \times \Omega_p, \\ T(t, x) &= T_{\text{body}} && \text{on } [0, \infty) \times \partial\Omega, \\ T(0, x) &= T_{\text{body}} && \text{in } \Omega. \end{aligned} \tag{2}$$

The equation models the constant temperature of the cooled probe by the corresponding Dirichlet condition. On the tissue surrounding the computational volume Ω we assume the temperature to be fixed as well. Obviously we have to set the corresponding initial condition $T(0, x)$ at the beginning of the treatment. The parameter $\lambda(x)$ denotes the heat-conductivity of the involved materials. In this general model the source-sink term on the right hand side consists of

$$q(t, x) := \sigma(x)|\nabla P(x)|^2$$

which is the heat source due to the resistance of the tissue to the electric current induced by the potential P .

Further effects

There are a couple of (bio-)physical effects which we have not considered in our model above. First, we have neglected the phase changes of water and nitrogen: Already at temperatures lower than 100°C the vaporization of nitrogen influences the energy balance. We neglect the metabolism and phase changes of proteins as well. A physically correct approach would take this effect into account using a multi-phase model. Such an improved model is subject of our work in progress.

We consider the tissue being destroyed as soon as it is exposed to a critical temperature $T_{\text{crit}} = 54^\circ\text{C}$. But already at lower temperatures protein denaturation begins. This can be taken into account by the Arrhenius formalism [Arr87] in which the applied temperature is integrated over time.

3 Modelling of perfusion

Pennes' approach

In the well known and widely used approach based on the formalism of Pennes [Pen48] the perfusion is modeled as a heat-sink term on the right hand side of the bioheat-transfer equation. For vessels with diameter $d < 2\text{mm}$ the Pennes model is accepted to be realistic, however for larger vessels the blood perfusion cannot be considered being purely diffusive any more. We generalize the right hand side of the equation to

$$q(t, x) := \sigma(x)|\nabla P(x)|^2 + \nu(x)k(x)(T_{\text{body}} - T(t, x))$$

where the parameter $\nu(x)$ gives the relative perfusion. It is set to a larger value within the vascular structures Ω_v as in the functional tissue Ω_t . In the quantity $k(x)$ we have collected the density of blood and tissue and the heat capacity of blood for reasons of simplicity.

Jain's approach

Next, we consider the approach due to Jain [JGG79] which changes the thermal conductivity toward an effective thermal conductivity. We define

$$\lambda_{\text{eff}}(x) = \lambda(x)(1 + \sqrt{\nu(x)}),$$

where ν is the relative perfusion coefficient from above. This approach consider perfusion to be purely diffusive similar to the Pennes approach above.

Dirichlet boundary condition

Finally, we consider the blood temperature in large vessels to be constant at body-temperature. If the vessels are large enough this approach should be realistic. However for smaller vessels the blood-temperature will increase significantly and not be constant at T_{body} . In the PDE (2) we model this approach with the additional boundary condition

$$T(t, x) = T_{\text{body}} \quad \text{in } [0, \infty) \times \Omega_\nu.$$

4 Temporal discretization

Let us now describe the discretization of the model. In the following sections we do not focus on the particulars of the perfusion modelling. Instead we assume that λ and $q(t, x)$ are chosen appropriately.

First we show, how the parabolic initial value problem (2) is transformed into a sequence of elliptic problems (like (1)). To this end we introduce a temporal grid-width τ and divide the time-axis into equidistant intervals of length τ . We denote the grid-points of this temporal grid with $T^n(x) := T(n\tau, x)$ for $n \in \mathbb{N}$ and such that $T^n : \Omega \rightarrow \mathbb{R}$.

Since from the viewpoint of treatment planning our interest lies mainly in the steady states of the therapy, i.e. the state in which the temperature-distribution does not change any more, we are using an implicit temporal scheme which allows us to choose τ large. Thus, we replace the temporal derivative $\partial_t T$ with a backward difference quotient

$$\delta_t^-(n\tau) = \frac{T^n - T^{n-1}}{\tau}$$

and evaluate the right hand side (and all nonlinearities, if we are working with the full nonlinear model) at the old time-steps T^{n-1} . The resulting time-discrete scheme then reads

For each time step $n \in \mathbb{N}$ find $T^n : \Omega \rightarrow \mathbb{R}$ such that $T^0 \equiv T_{\text{body}}$ and

$$\begin{aligned} \tau^{-1}(T^n(x) - T^{n-1}(x)) - \text{div}(\lambda(x)\nabla T^n(x)) &= q(n\tau, x) && \text{in } \Omega, \\ T^n(x) &= T_{\text{probe}} && \text{in } \Omega_p, \\ T^n(x) &= T_{\text{body}} && \text{on } \partial\Omega, \\ [T^n(x) &= T_{\text{body}} && \text{in } \Omega_\nu]. \end{aligned} \quad (2T)$$

Thus, the parabolic problem has been transformed into a sequence of elliptic problems similar to (1), which can be discretized in space as shown in the next paragraphs.

5 Spatial discretization

Let us now proceed with the discretization of the elliptic problems (1) and (2T). By the usual operations, we can transform these inhomogeneous boundary value problems into homogeneous ones, i.e. with zero boundary conditions on Γ^\pm , $\Omega_p \cup \partial\Omega$, or $\Omega_p \cup \partial\Omega \cup \Omega_v$, respectively. We denote the resulting right hand side with r_1 respectively r_2 .

We define a uniform hexahedral grid \mathcal{M}^h on Ω , where h is the width of the grid-elements $E \in \mathcal{M}^h$. Furthermore we denote the nodes of the grid (lying at the intersections of grid-lines) with x_j . The standard finite element space over \mathcal{M}^h in which the approximate solutions P_h and T_h^n of (1) and (2T), respectively, shall be contained consists of all functions which are piecewise trilinear on the elements E , i.e.

$$\mathcal{V}^h := \{v_h : \Omega \rightarrow \mathbb{R} : v_h \text{ is continuous, } v_h|_E \text{ is trilinear for all } E \in \mathcal{M}^h\}.$$

A basis of \mathcal{V}^h is given by the well known hat functions ϕ_i , which are characterized by

$$\phi_i(x_j) = \delta_{ij}, \quad \text{and} \quad \phi_i|_E \text{ is trilinear.}$$

By multiplying our problem-equations with test functions $\phi_j \in \mathcal{V}^h$, integrating over Ω and applying Green's formula we obtain the weak form of the above partial differential equations. The Neumann boundary conditions arise naturally from the weak form, whereas the Dirichlet boundary conditions have to be coded into the space \mathcal{V}^h . Denoting the L^2 scalar product over Ω with $(v, w) := \int_\Omega vw \, dx$ we can write the weak form for the computation of the potential as:

<p style="margin: 0;"><i>Find $P_h \in \mathcal{V}^h$ such that for all $\phi_j \in \mathcal{V}^h$</i></p> $(\sigma \nabla P_h, \nabla \phi_j) = (r_1, \phi_j) \tag{1S}$
--

And similarly for the computation of the heat distribution:

<p style="margin: 0;"><i>Find $T_h^n \in \mathcal{V}^h$ such that for all $\phi_j \in \mathcal{V}^h$</i></p> $(T_h^n, \phi_j) + \tau (\lambda \nabla T_h^n, \nabla \phi_j) = (r_2, \phi_j) \tag{2S}$
--

Inserting the basis decomposition of $P_h(x) = \sum p_i \phi_i(x)$ and similarly $T_h^n(x) = \sum t_i \phi_i(x)$ we arrive at systems of linear equations for the coefficients p_i respectively t_i :

$$M_1(p_1, \dots, p_N)^T = r_1, \quad M_2(t_1, \dots, t_N)^T = r_2,$$

which can be solved by a standard iterative method like Gauß-Seidel or CG. However, in the applications shown below we used a multigrid solver which has much better convergence properties as the before mentioned ones.

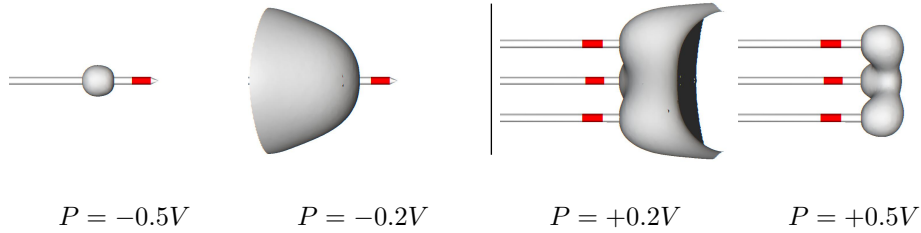


Figure 2: Iso-surfaces of the potential P from one respectively three bipolar RF-probes.

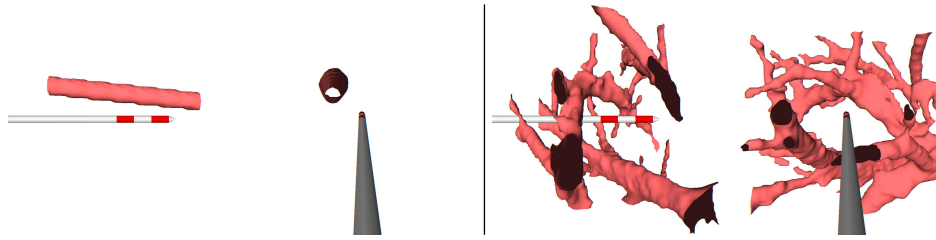


Figure 3: On the left the position of the artificial vessel and the bipolar probe is shown from two different viewpoints. On the right the same viewpoints show the configuration for the real vascular data.

6 Applications and comparison

In this section we apply the RF simulation model and compare the results of the different perfusion modelling approaches. We use a test-setting which consists of a single artificial vessel of diameter $d = 3$ mm and a setting in which we have extracted the vascular data from a real CT-data-set [ZJE⁺95, SPP00].

Our model approach from above has no restrictions on the size, number and position of the RF-probes. Therefore we can simulate settings as well in which more probes are used simultaneously. In Figure 2 iso-surfaces of the potential resulting from the RF-probe are shown. We show a setting with one probe as well as a setting with three similar probes. Since the heat-source for equation (2) is given by the gradient of the potential, it is highest in the middle of the probes where the electrodes face each other.

In Figure 3 we show the position of the RF-probe relative to the artificial respectively real vascular structure. In the Figures below we show only one of the perspectives to illustrate the shape of the temperature iso-surfaces relative to the vessels.

The application of the models to the artificial vessel data-set is shown in Figure 4. It is clearly visible from the images how far the $325K$ iso-surface (for which we can consider the tissue being destroyed) is away from the vessel. In this application the Jain-model gives the iso-surfaces closest to the vessel, whereas the Pennes approach and clearly the Dirichlet condition prevents the temperature from surrounding the vessel. In Figure 5 we have

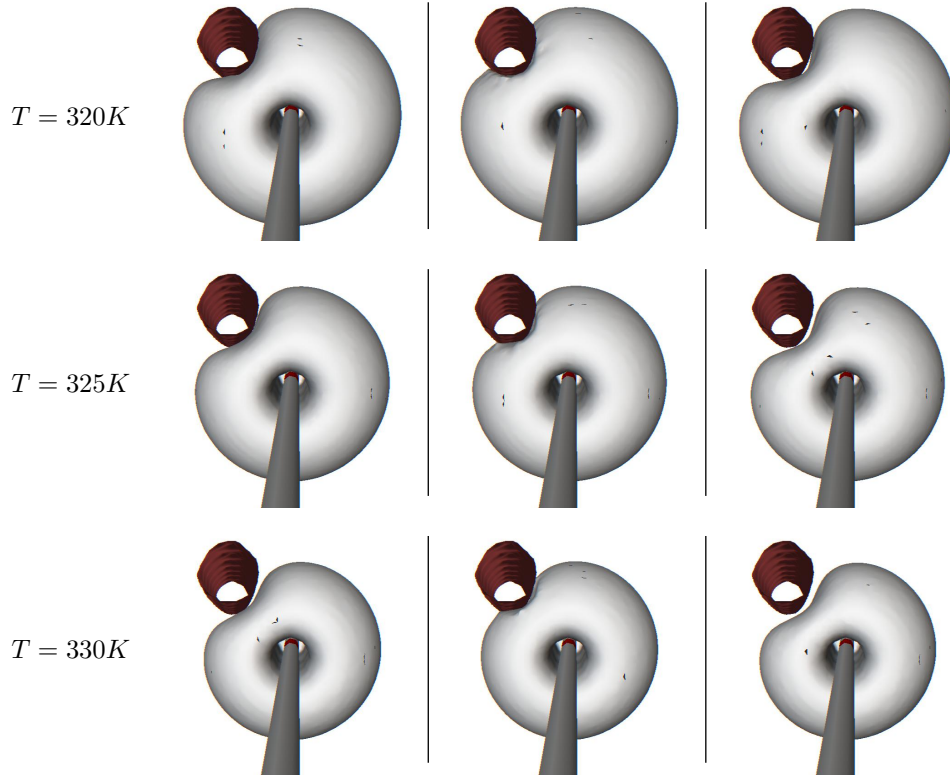


Figure 4: Results from the sample configuration. Iso-surfaces of the temperature distribution after $t = 5$ min are shown. In the left column the Pennes approach was used, in the middle column we used the approach due to Jain. In the right column Dirichlet boundary conditions have been set inside the vessel.

depicted the results from the application to the real data-set. Again we see that the temperatures from the Jain approach surrounds the vessels best. The Dirichlet-model gives the $325K$ heat iso-surface which is the furthest away from the vessel.

For all computations we used a grid resolution of $65 \times 65 \times 65$ and a corresponding grid-size $h = 10^{-3}$. Since we use an implicit time-discretization there is no restriction to the time-step width τ and so we used a time-step of $\tau = 10$ secs. The other parameters used for all computations were $T_{\text{body}} = T_{\text{probe}} = 310$ K, $\lambda = 0.471$ W/(mK), $\sigma = 0.167$ S/m, $k = 1182$ and $\nu_{\text{tissue}} = 10^{-14}$ 1/s, $\nu_{\text{vessel}} = 10^{-4}$ 1/s. The generator had a power of 100 W.

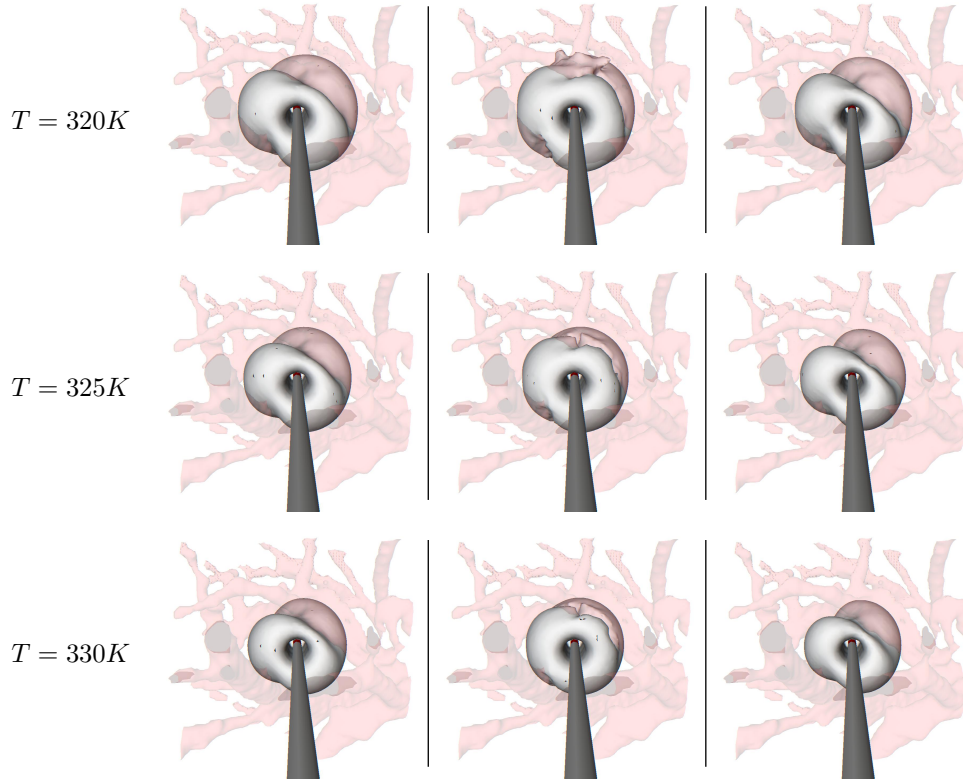


Figure 5: Results from the real vascular data set. Again iso-surfaces of the temperature distribution after $t = 5$ min are shown. Left column: Pennes, middle column: Jain, right column: Dirichlet. To emphasize the shape the temperature iso-surfaces relative to the vessel we have drawn the vascular structures transparent.

7 Conclusions and future work

We have discussed a model for the simulation of RF-ablation and three different approaches to the modelling of perfusion. Results have been shown for an artificial setting and a setting resulting from real CT-data. To summarize the results we note that the Dirichlet approach behaves bad for small vessels, since we can assume the temperature to be close to body temperature only for large vascular structures. On the other hand, the Pennes approach is known to give good results for capillary blood perfusion only [Ste00, Pen48]. The approach due to Jain gives a $325 K$ iso-surface, which is very close to the vessels. This does not seem realistic for large vessels as well. The comparison of our results to real ablations or temperature measurements is work in progress.

As we have already described above, for large vessels the perfusion can not be considered diffusive any more. Therefore we are working on a generalization of the models toward

a transport diffusion approach for the heat-distribution. Together with an improved spatial resolution [PPL⁺04] of the complicated geometric structures in the organ under consideration this should give a major advancement to the perfusion modelling.

On the web site www.mevis.de/~tp/rfitt more color figures and movies of the results can be found.

Acknowledgements

We acknowledge Dr. T. Stein and Dr. A. Roggan from Celon AG, Teltow for fruitful discussions on the RF-model. Furthermore we acknowledge the Group of Martin Rumpf from Duisburg University, whose numerics software package was used for the computations shown here.

References

- [Arr87] S. Arrhenius. *Über die Reaktionsgeschwindigkeit bei der Inversion von Rohrzucker durch Säuren*. Z. Phys. Chem., 4:226–248, 1887.
- [JGG79] R. K. Jain, F. H. Grantham and P. M. Gullino. *Blood flow and heat transfer in Walker 256 mammary carcinoma*. J. Natl. Cancer Inst., 69:927–931, 1979.
- [Pen48] H. H. Pennes. *Analysis of tissue and arterial blood temperatures in a resting forearm*. J. Appl. Physiol., 1:93–122, 1948.
- [PPL⁺04] T. Preusser, H.-O. Peitgen, F. Liehr, M. Rumpf, U. Weikard and S. Sauter. *Simulation of radio-frequency ablation using composite finite element methods*. In: Perspective in Image Guided Surgery, Proceedings of the Scientific Workshop on Medical Robotics, Navigation and Visualization, pp. 303–310, Remagen, 2004.
- [SPP00] A. Schenk, G. Prause and H.-O. Peitgen. *Efficient Semiautomatic Segmentation of 3D Objects in medical images*. In: Medical Image Computing and Computer-Assisted Intervention, MICCAI, volume 1935 of Springer LNCS, pp. 186–195, Pittsburgh, 2000.
- [Ste00] T. Stein. *Untersuchungen zur Dosimetrie der hochfrequenzstrominduzierten interstitiellen Thermotherapie in bipolarer Technik*. Nummer 22 in Fortschritte in der Lasermedizin. Müller, Berlin, LMTB, 2000.
- [TSHea02] Supan Tungjitkusolum, S. Tyler Staelin, Dieter Haemmerich and et al. *Three-dimensional Finite-Element Analyses for Radio-Frequency Hepatic Tumor Ablation*. IEEE Transactions on Biomedical Engineering, 49(1):3–9, 2002.
- [ZJE⁺95] C. Zahlten, H. Jürgens, C. J. G. Evertsz, R. Leppek, H.-O. Peitgen and K.-J. Klose. *Portal vein reconstruction based on topology*. European Journal of Radiology, 19:96–100, 1995.